Neural circuit repair by low-intensity magnetic stimulation requires cellular magnetoreceptors and specific stimulation patterns

T. Dufor, S. Grehl, A. Tang, M. Doulazmi, Massiré Traoré, N. Debray, C. Dubacq, Z.-D. Deng, J. Mariani, A. Lohof, et al.

NEUROSCIENCE

Neural circuit repair by low-intensity magnetic stimulation requires cellular magnetoreceptors and specific stimulation patterns

T. Dufor[1], S. Grehl[1,2], A. D. Tang[2], M. Doulazmi[1], M. Traoré[3], N. Debray[1], C. Dubacq[4], Z.-D. Deng[5], J. Mariani[1,6], A. M. Lohof[1], R. M. Sherrard[1,6]*

Although electromagnetic brain stimulation is a promising treatment in neurology and psychiatry, clinical outcomes are variable, and underlying mechanisms are ill-defined, which impedes the development of new effective stimulation protocols. Here, we show, in vivo and ex vivo, that repetitive transcranial magnetic stimulation at low-intensity (LI-rTMS) induces axon outgrowth and synaptogenesis to repair a neural circuit. This repair depends on stimulation pattern, with complex biomimetic patterns being particularly effective, and the presence of cryptochrome, a putative magnetoreceptor. Only repair-promoting LI-rTMS patterns up-regulated genes involved in neuronal repair; almost 40% of were cryptochrome targets. Our data open a new framework to understand the mechanisms underlying structural neuroplasticity induced by electromagnetic stimulation. Rather than neuronal activation by induced electric currents, we propose that weak magnetic fields act through cryptochrome to activate cellular signaling cascades. This information opens new routes to optimize electromagnetic stimulation and develop effective treatments for different neurological diseases.

INTRODUCTION

Our imperfect understanding of the extraordinarily complex human brain means that repairing neuronal damage or dysfunction remains one of the major challenges in biomedical science. Noninvasive brain stimulation (NIBS) is increasingly used in neurology and psychiatry, aiming to trigger intrinsic brain repair mechanisms. While clinical outcomes are promising, they are variable between subjects and studies and often not reproducible (*1*, *2*). Because the mechanisms underlying different NIBS approaches are poorly understood, the development of appropriate therapeutic protocols for different neurological diseases is by trial and error rather than systematic adjustment of a stimulation protocol that targets the underlying pathology (*1*).

A commonly used NIBS protocol uses electromagnetic stimulation in one of two forms: (i) repetitive transcranial magnetic stimulation (rTMS) delivering strong electromagnetic pulses [0.5 to 2 Tesla (T)], which induce strong electric fields in the underlying brain tissue that depolarize neurons and trigger activity-dependent neuronal plasticity (*1*); or (ii) low-/pulsed-field magnetic stimulation involving weak pulses [microtesla (μT) to millitesla (mT)] delivered to the whole brain, which induce weak subthreshold electric fields that modulate function without direct neuronal firing (*3*, *4*). The effects of electromagnetic stimulation depend on stimulation frequency, pattern, duration, and number of pulses delivered (*1*). These are restricted in high-intensity rTMS for technical reasons (heating) and safety considerations [pain and seizures; (*2*)]. In contrast, low-field stimulation uses a wide range of frequencies and patterns to modulate neuronal excitability (*3*, *5*), neuroplasticity (*6*), neuron survival (*7*, *8*), and calcium signaling (*9*). Nevertheless, it is unknown how these weak fields induce their diverse physiological effects. Is a specific dose (number of pulses) required? Is the frequency/pattern of pulse delivery important? Since these fields are too weak to trigger neural firing, does the magnetic component of the electromagnetic field affect neurons directly?

To address these questions and identify mechanisms underlying low-field electromagnetic stimulation, we developed focal low-intensity (in the mT range) repetitive transcranial magnetic stimulation (LI-rTMS), i.e., low-intensity magnetic fields delivered focally to only part of the brain such as rTMS, while maintaining the safety and frequency range of low-field stimulation (*4*). Using LI-rTMS, we have shown that complex biomimetic high-frequency stimulation (BHFS) increases intracellular calcium, and brain-derived neurotrophic factor (BDNF) modifies neuronal gene expression and prunes abnormal connections in the mouse visual system (*10*–*12*). However, the link between the electromagnetic field and cellular signaling (e.g., BDNF), as well as between the stimulation dose or pattern and the structural neural circuit changes, remains unknown. We tested different LI-rTMS protocols (frequency and pattern) and the involvement of the magnetic field (in the presence or absence of a potential magnetoreceptor, cryptochrome) using an experimental model in which a biological effect can be readily quantified: postlesion repair in the mouse olivocerebellar path.

Here, we report that LI-rTMS (10 min/day for 2 weeks) induces postlesion axonal outgrowth and olivocerebellar reinnervation in vivo and ex vivo. This repair critically depends on the stimulation pattern, with complex biomimetic frequencies being more effective than the regular rhythms that are usually used in human rTMS (*1*, *2*). We show that LI-rTMS requires cellular cryptochrome magnetoreceptors to induce reinnervation and modulates cryptochrome target genes involved in axon growth and regeneration (*13*–*16*). These data demonstrate that magnetic fields themselves can modify the brain without needing to directly activate neuronal firing, information that will facilitate the

[1]Sorbonne Université and CNRS, IBPS, UMR 8256 Biological Adaptation and Ageing, Paris, France. [2]Experimental and Regenerative Neuroscience, School of Animal Biology, University of Western Australia, Perth, Australia. [3]Inovarion, F-75013 Paris, France. [4]Sorbonne Université, IBPS, CNRS UMR 8246 and INSERM U1130 Neuroscience Paris Seine, Paris, France. [5]Noninvasive Neuromodulation Unit, Experimental Therapeutics and Pathophysiology Branch, Intramural Research Program, National Institute of Mental Health, National Institutes of Health, Bethesda, MD, USA. [6]Sorbonne Université and Assistance Publique Hôpitaux de Paris, Institut de la Longévité, Charles Foix Hospital, Ivry-sur-Seine, France.
*Corresponding author. Email: rachel.sherrard@sorbonne-universite.fr

development of new noninvasive treatment strategies for human neurological disease.

RESULTS

LI-rTMS induces olivocerebellar reinnervation in vivo

We previously demonstrated that after unilateral olivocerebellar lesion (pedunculotomy), which removes all climbing fibers (olivocerebellar axon terminals) from a hemicerebellum, intracerebellar injection of certain neurotrophic factors induces remaining inferior olive neurons to extend axon collaterals and partially reinnervate the denervated cerebellar Purkinje cells (*17*, *18*). Because LI-rTMS increases BDNF (*11*, *12*), we tested whether it could replace the invasive neurotrophic factor injection and induce olivocerebellar reinnervation. As proof of concept, we used our established BHFS protocol (10 min/day for 2 weeks) (*11*, *12*) to stimulate the cerebellum of 3-month-old male mice after pedunculotomy (Fig. 1, E and F). Sham stimulation did not induce any reinnervation (Fig. 1B). In contrast, BHFS produced vesicular glutamate transporter 2 (VGLUT2)–positive terminals in the molecular layer of the left hemicerebellum (Fig. 1, C and D), organized in parasagittal arbors [compare Fig. 1 (A and B, RHCbm) and Fig. 1 (C and D)] identical to normal climbing fibers (*19*) and those induced by BDNF (*17*, *18*). Labeling extended into the vermis and paravermis and sparsely into the lateral hemisphere (Fig. 1G).

LI-rMS induces Purkinje cell reinnervation ex vivo in a pattern-dependent manner

Climbing fiber reinnervation in vivo (Fig. 1) indicates that BHFS LI-rTMS can promote axonal outgrowth. Because reinnervation was incomplete, we systematically tested other LI-rTMS patterns for possible greater effects. To accelerate the screening of different repetitive magnetic stimulation at low intensity (LI-rMS, as it is not "transcranial") patterns, we used our ex vivo model of olivocerebellar pathway pedunculotomy, denervated cocultured hindbrain explants (Fig. 2A and fig. S1), in which intact host climbing fibers grow collaterals into the graft to reinnervate (VGLUT2-positive terminals) the Purkinje cell soma and primary dendrites (Fig. 2B and fig. S1).

As in vivo, BHFS induced reinnervation ex vivo (Fig. 2C). We then tested frequencies used in human rTMS for facilitation [10 Hz and intermittent theta burst stimulation (iTBS)] or inhibition [1 Hz and continuous theta burst stimulation (cTBS)] of cortical excitability (*1*). LI-rMS with the complex iTBS pattern significantly increased reinnervation (Fig. 2C), similar to BHFS, whereas the constant 10-Hz stimulation was less effective, inducing reinnervation only to the proximal zone (Fig. 2C). In each group, VGLUT2 labeling was greater near the host explant (proximal zone) and decreased with distance from the host-graft interface (Fig. 2C). However, intergroup differences persisted in both proximal and distal zones. In contrast, 1 Hz and cTBS did not induce more reinnervation than occurred in sham controls (Fig. 2C).

Next, we tested whether the efficacy of complex pattern LI-rMS depended on the number of pulses delivered. We found that reinnervation density did not correlate with the number of stimulation pulses (Pearson coefficient, $P = 0.353$; Fig. 2, D and E); however, stimulation pattern was also changed between groups, which confounds interpretation of the results. Therefore, we tested our hypothesis by creating a randomized iTBS (R-iTBS), a stimulation pattern that delivers the same number of pulses as iTBS (1800 per session; Fig. 2E) in the same number of high-frequency 50-Hz bursts but repeats them randomly (2 to 60 Hz) in the 2 s of stimulation (fig. S1E) rather than at the theta rhythm (5 Hz). Two weeks' R-iTBS failed to induce reinnervation (Fig. 2C), indicating the importance of the theta rhythm for the induction of reinnervation.

We also examined the role of the stimulation target: Did reinnervation require stimulation of both the cerebellum (reinnervation targets) and the inferior olive (afferent reinnervating neurons), or only one of these? This question is clinically important because stimulation of a whole system is not always feasible, for example, the motor cortex and the spinal cord. To address this issue, we shielded either the cerebellar or brainstem portion of the explant with mu-metal (see Materials and Methods) during daily BHFS LI-rMS. Neither protocol induced significant reinnervation (Fig. 3A). The apparent need for LI-rMS to both inferior olive and cerebellum differs from in vivo, where the inferior olive receives much weaker LI-rTMS than the cerebellar cortex. Because mu-metal shielding acts largely through deflection of the electromagnetic field (*20*), we checked the field intensities arriving at the exposed parts of the explant. Modeling revealed that the edge of the mu-metal deflected the magnetic field direction by approximately 45°, so that it was no longer perpendicular to the explant. This direction tilt reduced the peak field magnitude at the exposed tissue by approximately 50% (Fig. 3, B and C), which is consistent with less reinnervation. We confirmed that reduced LI-rMS intensity could explain the lack of reinnervation by stimulating whole explants with 4.5 mT (the value identified in the modeling; $n = 5$) and observed that only 8.2 ± 1.6% Purkinje cells were reinnervated by climbing fibers, which is not significantly different from sham, cerebellar-only stimulation, or olivary-only stimulation [analysis of variance (ANOVA) with Tukey post hoc; sham, $P = 0.99$; cerebellum, $P = 0.52$; inferior olivary nucleus (ION), $P = 0.37$]. Given the differential stimulation doses in vivo (cerebellum > inferior olive) and the lack of additive effect when both cerebellum and inferior olive receive the lower 4.5-mT dose, these data suggest that LI-rMS to the target cerebellum must be above a baseline intensity to induce olivocerebellar reinnervation.

Together, these studies show that LI-rMS can induce axonal outgrowth and olivocerebellar reinnervation and reveal that stimulation frequency and pattern, rather than overall pulse number, determine the effect. In addition, similar reinnervation induced by very different stimulation protocols (e.g., BHFS and iTBS) and the completely dissimilar effects of almost identical protocols (iTBS and R-iTBS) indicate that the observed reinnervation is due to LI-rMS, not nonspecific heat or vibration that can occur with magnetic stimulation, although not detectable in our system (*20*). The data also suggest that stimulation to the target cerebellar tissue must be above a minimum intensity to induce axonal outgrowth and reinnervation.

LI-rMS modulates growth-promoting genes in the cerebellum

To identify potential mechanisms by which LI-rMS brings about neural repair, we examined cerebellar protein and gene expression at an early stage of stimulation, i.e., before (c-fos) and during (gene expression) the process of reinnervation. First, we identified population(s) of cerebellar cells responding to the stimulation by immunolabeling of the immediate-early gene c-fos (2.5 hours after a single session of LI-rMS). We observed c-fos–positive cells throughout the graft plates with no apparent concentration in zones that would later become innervated (fig. S2). BHFS or R-iTBS doubled the number of c-fos–positive cells (821.3 ± 79.7/mm^2 and 980.8 ± 110/mm^2, respectively) compared with

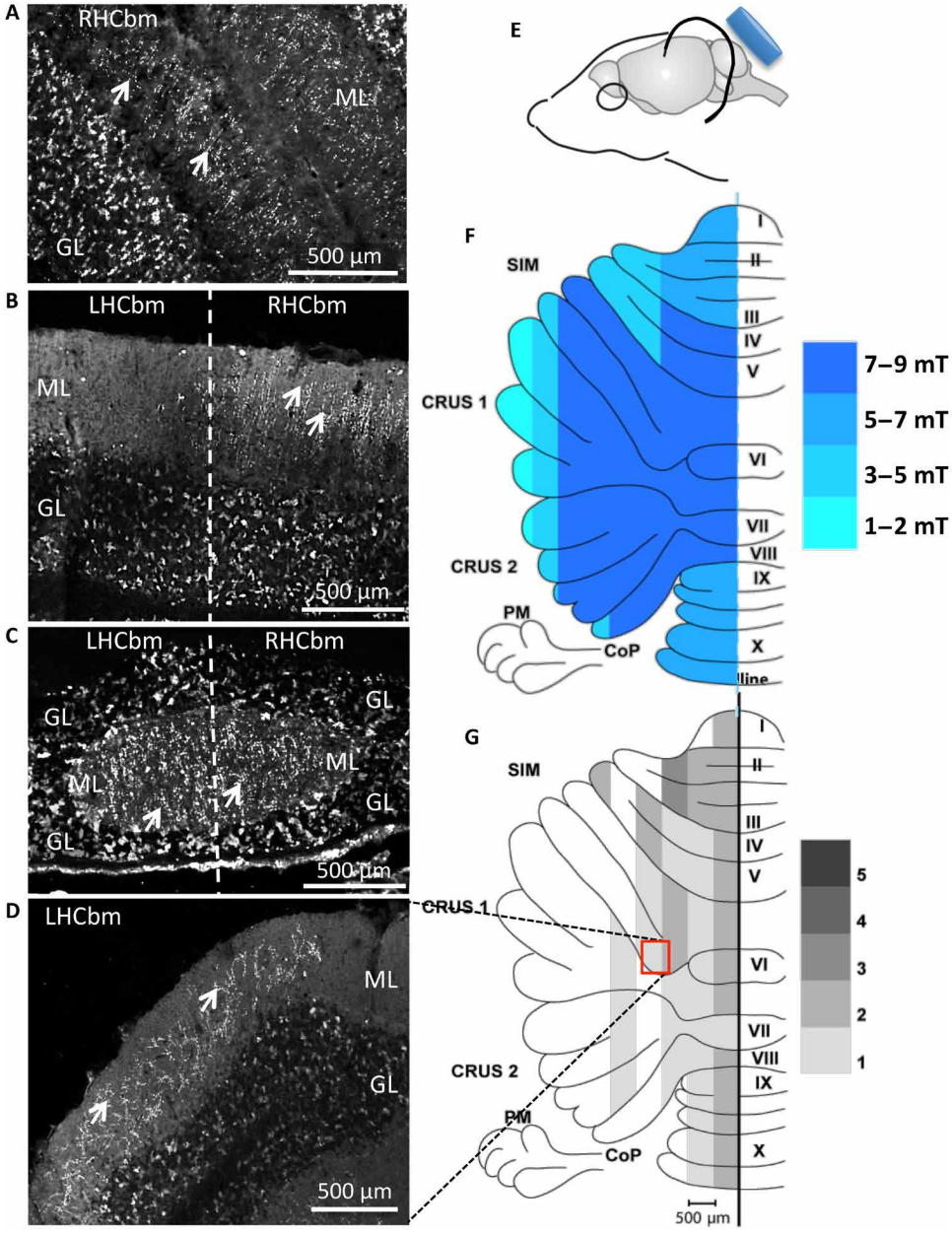

Fig. 1. LI-rTMS induces transcommissural climbing fiber reinnervation in pedunculotomized adult mice. (**A**) Climbing fibers (white arrows) in the molecular layer (ML) of the intact right hemisphere (CRUS 1 and CRUS 2 coronal sections) from a sham-treated mouse ($n = 5$). (**B**) After sham treatment, in coronal sections, VGLUT2-positive climbing fibers (white arrows) in the molecular layer of the right hemicerebellum stop at the midline (thick vertical dashed line), consistent with lack of reinnervation (*18*). (**C**) In comparison after LI-rTMS ($n = 9$), VGLUT2-positive climbing fibers (white arrows) fill the molecular layer on both sides of the midline (thick vertical dashed line) in this coronal section, consistent with reinnervation. (**D**) Further laterally, VGLUT2-positive climbing fibers (white arrows) in the molecular layer of the lesioned hemisphere following LI-rTMS. Anatomical differences from (A) and (B) reflect the noncoronal orientation of the lobule (simplex), and therefore, climbing fiber arbors are angled to the coronal plane of the section. (**E**) Diagram showing the coil (blue) in relation to the mouse head. (**F**) Unfolded cerebellum showing magnetic field intensity delivered by LI-rTMS, as measured by a Hall device in air at corresponding *X*, *Y*, and *Z* distances from the center of the coil. (**G**) Average density, in 0.5-mm parasagittal zones, of LI-rTMS–induced climbing fiber reinnervation ($n = 9$). This parasagittal organization of different reinnervation densities is consistent with that previously demonstrated in BDNF-induced climbing fiber reinnervation, which demonstrates parasagittal topography and provides recovery of motor and navigation behaviors (*18*). Grayscale grading: 1 = few strands; 2 = one-quarter lobule; 3 = half lobule; 4 = three-quarter lobule; and 5 = completely climbing fiber–filled (*18*). GL, granular layer; LHCbm, left hemicerebellum; RHCbm, right hemicerebellum; SIM, lobulus simplex; PM, paramedian lobule; CoP, copula pyramidis; I to X, lobules 1 to 10 of the vermis. Photo credit: A. D. Tang, University of Western Australia, Experimental and Regenerative Neuroscience Laboratory.

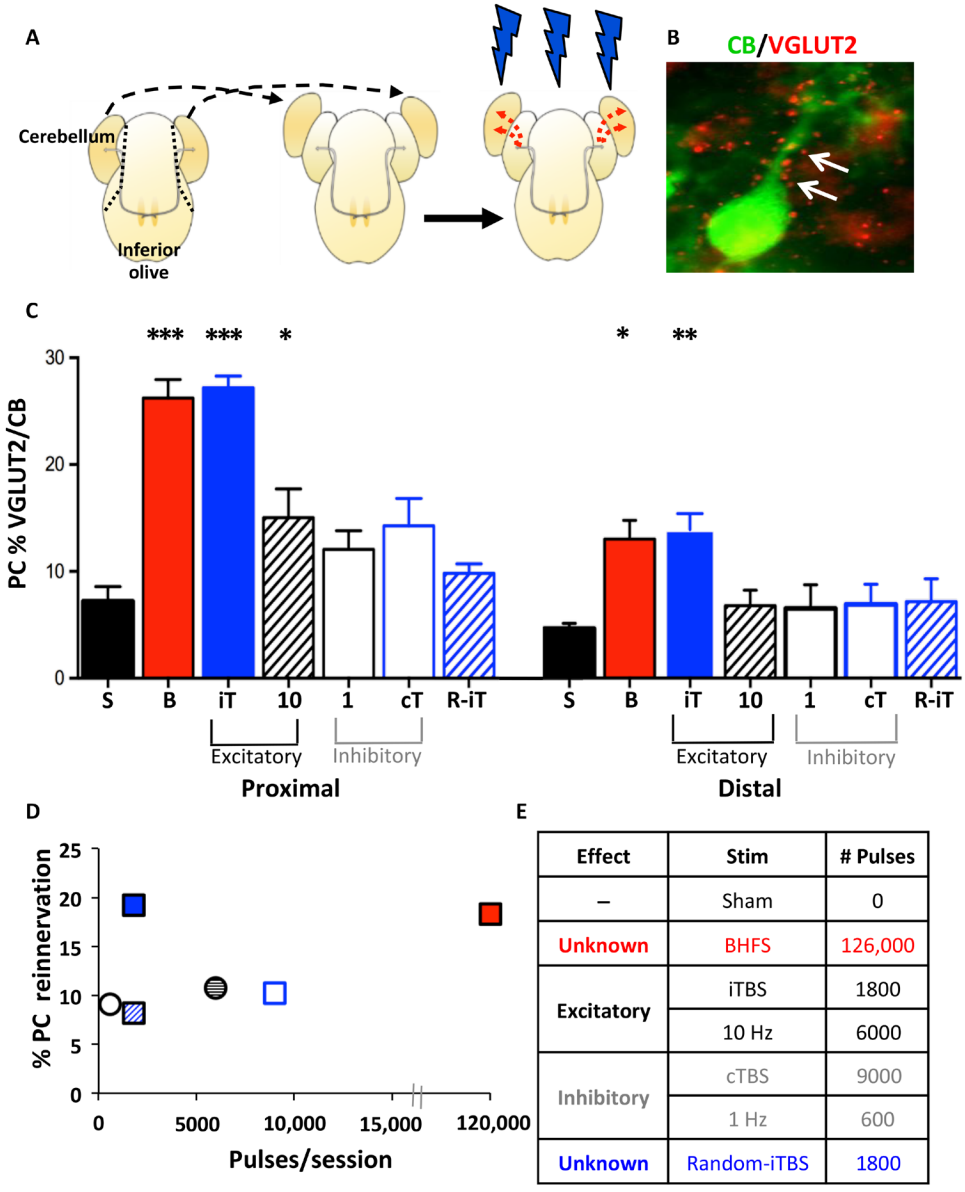

Fig. 2. LI-rMS pattern regulates climbing fiber reinnervation ex vivo. (**A**) Hemicerebella are removed from an explant (dotted line) and placed next to an intact explant (dashed arrows) for reinnervation (red dotted arrows) by host climbing fibers (thin gray arrows). ↯, LI-rMS (see fig. S1). (**B**) Purkinje cell (green) showing climbing fiber reinnervation (red puncta, arrows). Photo credit: R. M. Sherrard, Sorbonne Université, UMR8256 Biological Adaptation and Ageing. (**C**) Purkinje cell (PC) reinnervation is greater in proximal versus distal zones of the cerebellar plate [two-way repeated-measures analysis of variance (ANOVA), $P < 0.001$]. BHFS (B; $n = 11$) and intermittent theta burst stimulation (iTBS) (iT; $n = 8$) induced significant reinnervation in both zones compared with sham (S; $n = 10$; ANOVA with Tukey post hoc; proximal: BHFS and iTBS, both $P < 0.001$; distal: BHFS, $P = 0.003$; iTBS, $P = 0.002$). Ten hertz ($n = 8$) also induced Purkinje cell reinnervation proximally ($P = 0.048$), but not distally ($P = 0.96$), although less than iTBS and BHFS ($P < 0.001$). Excitatory and inhibitory indicate stimulus effects in high-intensity rTMS [see (E)]. One Hz (1; $n = 6$), continuous theta burst stimulation (cTBS) (cT; $n = 8$), and randomized iTBS (R-iTBS) (R-iT; $n = 7$) did not induce more reinnervation than sham (proximal: 1 Hz, $P = 0.577$; cTBS, $P = 0.097$; R-iTBS, $P = 0.952$; distal: 1 Hz, $P = 0.98$; cTBS, $P = 0.95$; R-iTBS, $P = 0.93$). Bars = means ± SEM. *$P < 0.05$, **$P < 0.01$, ***$P < 0.001$. (**D**) Reinnervation density does not reflect the number of pulses delivered per 10-min session (Pearson coefficient, $P = 0.353$), although changes in patterns may also contribute to this effect. (**E**) Pulses delivered in 10 min for each stimulation parameter and their effects in high-intensity rTMS. ■, Sham; □, 1 Hz; ▨, 10 Hz; ■, BHFS; ■, iTBS; □, cTBS; ▨, R-iTBS.

sham (439.2 ± 43.1/mm^2; $P < 0.001$), whereas iTBS and cTBS produced only an intermediate increase (599.6 ± 64.1/mm^2 and 567.6 ± 82/mm^2, respectively; $P > 0.05$; Fig. 4, A and B). Thus, there was no obvious correlation between either the numbers of pulses delivered (iTBS versus R-iTBS) or excitatory/inhibitory stimulation (iTBS versus cTBS) and the percentage of cells expressing c-fos (Fig. 4C).

However, when we only considered the target cells of climbing fiber reinnervation, Purkinje cells, and GABAergic interneurons, BHFS and iTBS similarly increased the fraction of cells that was

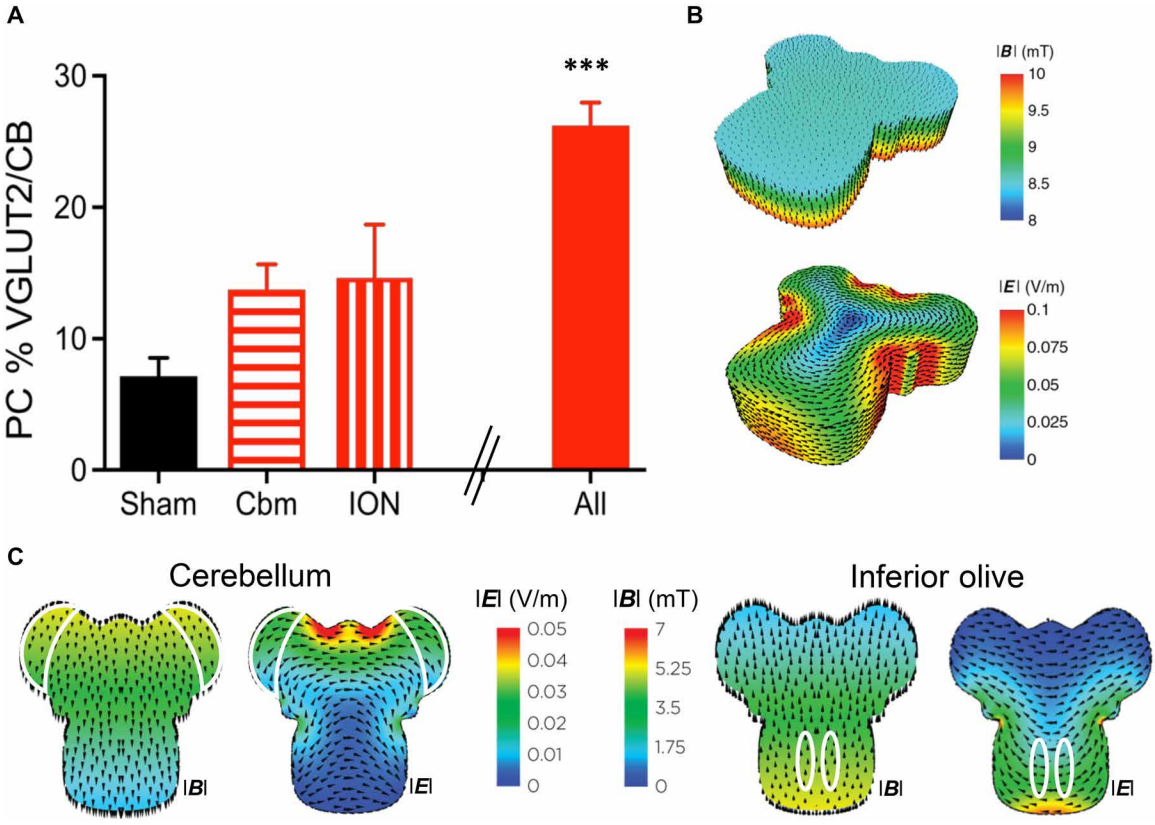

Fig. 3. LI-rMS intensity has a lower limit below which reinnervation fails. (**A**) BHFS stimulation of either the rostral [cerebellum (Cbm); $n = 4$] or the caudal (ION; $n = 4$) part of the explant does not induce significant reinnervation compared with sham (ANOVA with Tukey post hoc; cerebellum: $P = 0.20$; ION: $P = 0.12$). "All" is for comparison, showing reinnervation induced by BHFS (***$P < 0.001$) to the whole explant (Fig. 2). (**B**) Distribution of the magnetic (|***B***|; top) and electric (|***E***|; bottom) fields in the explant without shielding [reproduced from (*20*) with permission]. (**C**) Distribution of the modeled electric field (|***E***|) and magnetic field (|***B***|) in the explant when the caudal part is shielded ("cerebellum"; left) or when the rostral part is shielded ("ION"; right) from the LI-rMS coil. Arrowheads indicate the direction of the induced current flow or magnetic flux, as appropriate; and solid white lines delineate the areas of interest for stimulation (cerebellar plates or inferior olives).

c-fos–positive (Fig. 4, A and D, and table S2), whereas cTBS and R-iTBS did not.

We then examined the expression of genes associated with neurotrophin signaling, since neurotrophins can induce olivocerebellar reinnervation (*17*, *18*). We isolated RNA from the grafted cerebellar plate during the process of reinnervation (6 hours after the last of three daily LI-rMS sessions). We found significant changes in the expression of 10 genes (Fig. 4E) and likely changes in 12 other mRNAs (Fig. 4E and fig. S4). LI-rMS patterns that induced significant reinnervation (iTBS and BHFS) increased the expression of genes involved in Gene Ontology (GO) functions such as "axonogenesis, response to axon injury" (fig. S5 and table S3). In contrast, R-iTBS either did not change or reduced expression of other genes with the same GO functions (Fig. 4E, fig. S4, and table S3). The products of three genes whose expression was increased in iTBS and BHFS (Fig. 4E) are known to promote postlesion neuronal reinnervation in other neural systems: β_2-microglobulin (*B2m*), β-glucuronidase (*Gusb*), and neurotrophin-3/NT3 (*Ntf3*) (*14*–*16*).

Together, these data confirm our observations of reinnervation density (Figs. 2 and 3, top) that stimulation pattern determines the biological outcome. The two stimulation patterns that induce reinnervation, iTBS and BHFS, activate the same percentage of reinnervation targets (Purkinje cells and interneurons), despite activating different numbers of total cerebellar cells. They also up-regulate genes with the same GO biological function of axon outgrowth, although with some individual differences in the specific genes.

Cryptochrome is required for LI-rMS–induced postlesion repair

LI-rMS affects both neuroplasticity and gene expression, despite inducing an electric field in the explant tissue that is subthreshold for cerebellar neuron firing (*20*, *21*); therefore, we tested whether the magnetic field itself contributes directly to the LI-rMS effects. We rejected blocking electrical activity in the explant, as this would generate widespread nonspecific effects and not answer the question. Instead, we compared cerebellar reinnervation in explants from wild-type (WT) mice and mice deficient for the presumed magnetoreceptor, cryptochrome double knockout (DKO) ($Cry1^{-/-}Cry2^{-/-}$), which do not display overt cerebellar abnormality [fig. S3; (*22*)]. In *Drosophila*, light-activated cryptochrome mediates static magnetic field increase in neuronal excitation (*23*, *24*), although its response to pulsed magnetic fields is much less studied (*25*). However, it is unknown whether mammalian Cry acts as a light-independent magnetoreceptor in the brain.

In denervated cocultured explants from $Cry1^{-/-}Cry2^{-/-}$ DKO mice, 2 weeks daily BHFS failed to induce reinnervation (Fig. 5). To verify that this was not an inherent abnormality resulting from the cryptochrome deletion, we tested whether denervated $Cry1^{-/-}Cry2^{-/-}$ explants could respond to BDNF. Cryptochrome DKO explants

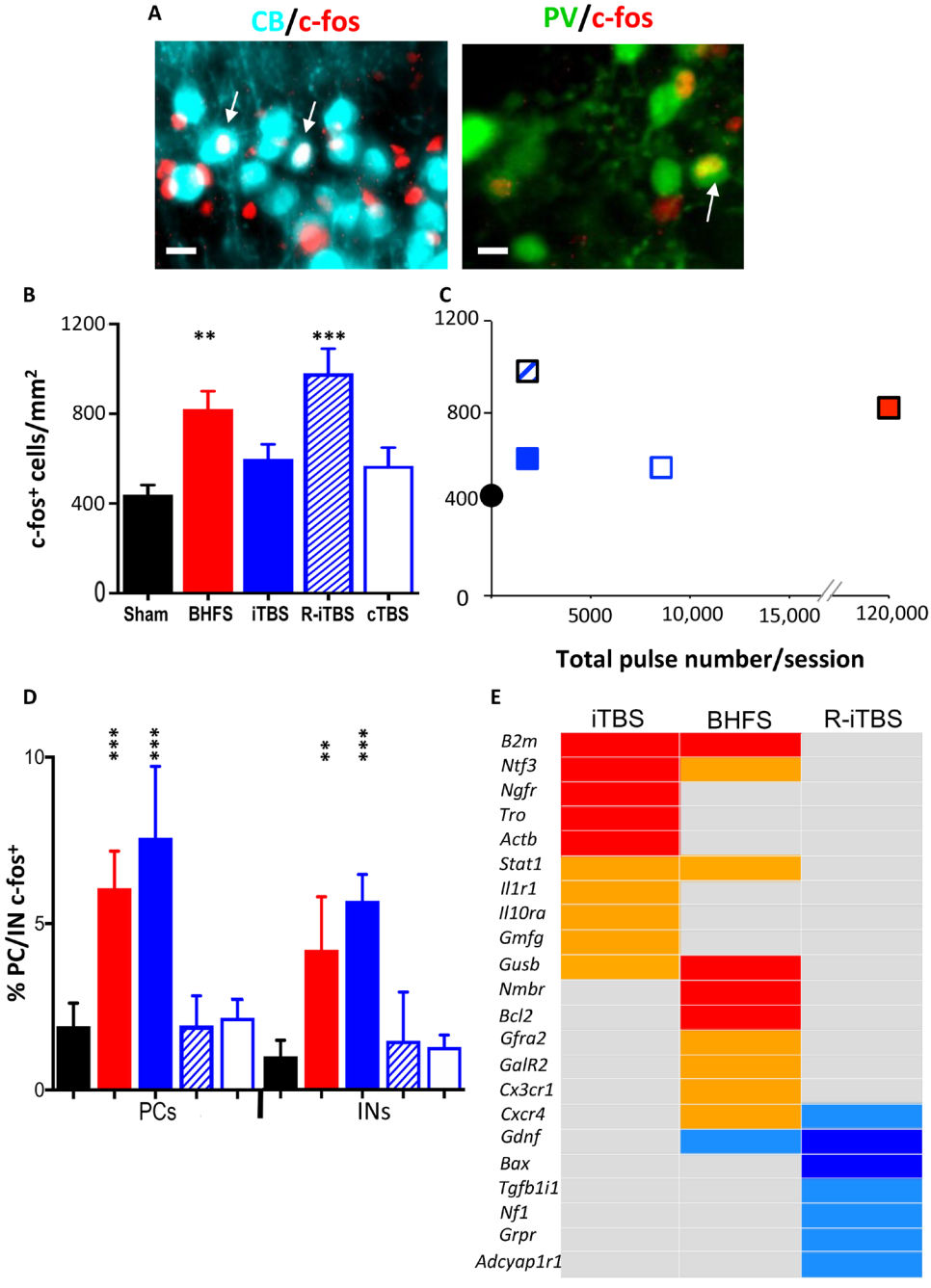

Fig. 4. LI-rMS modulates gene expression in denervated hemicerebellar plates. (**A**) c-fos (red) in Purkinje cell (cyan) and GABAergic (GABA-releasing) interneuron (green) nuclei (arrows). Scale bars, 20 μm. Photo credit: T. Dufor, Sorbonne Université, UMR 8256 Biological Adaptation and Ageing. PV, parvalbumin. (**B**) c-fos–positive profiles per square millimeter (means ± SEM) in sham ($n = 8$), BHFS ($n = 6$), iTBS ($n = 9$), R-iTBS ($n = 4$), or cTBS ($n = 7$) hemicerebella (ANOVA and Tukey post hoc comparison, $F_{4,29} = 7.3$, $P < 0.001$; compared to sham: BHFS, $P = 0.001$; iTBS, $P = 0.16$; R-iTBS, $P < 0.001$; cTBS, $P = 0.68$). (**C**) c-fos labeling does not reflect stimulation pulse number (Pearson coefficient, $P = 0.30$), although changes in patterns may also contribute to this effect; color codes are the same as in (B). (**D**) Percentage of calbindin- or parvalbumin-positive cells that are double-labeled c-fos/calbindin ("PCs") or c-fos/parvalbumin ("INs"; means ± SEM) in sham controls or after BHFS, iTBS, or R-iTBS (Fisher's exact test, compared with sham; BHFS: Purkinje cells, $P < 0.001$; interneurons, $P = 0.006$; iTBS: Purkinje cells, $P < 0.001$; interneurons, $P = 0.001$; R-iTBS: Purkinje cells, $P = 0.827$; interneurons, $P = 0.682$; cTBS: Purkinje cells, $P = 0.50$; interneurons, $P = 0.61$). (**E**) Heatmap showing expression changes of 22 genes from the mouse neurotrophins and receptors polymerase chain reaction (PCR) array after BHFS, iTBS, or R-iTBS. Red, up-regulated ($P < 0.05$); orange, strong trend for up-regulation ($0.05 < P < 0.1$); royal blue, down-regulated ($P < 0.05$); light blue, strong tend for down-regulation ($0.05 < P < 0.1$); gray, no change. CB, calbindin. Compared with sham, $^{**}P < 0.01$, $^{***}P < 0.001$. Color codes are the same as in (B).

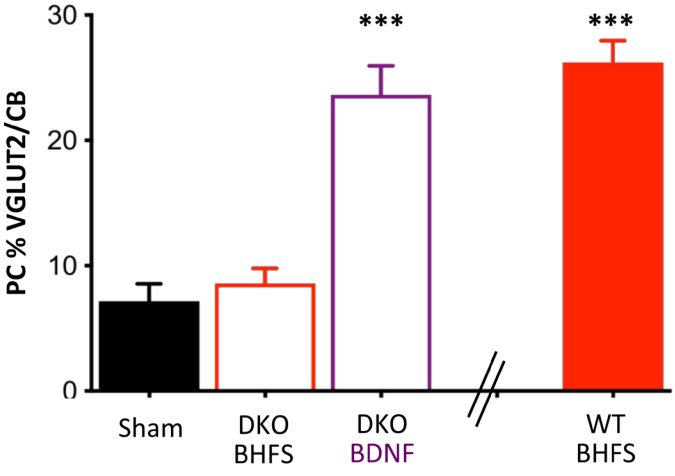

Fig. 5. Cryptochromes are required for LI-rMS–induced postlesion repair. Percentage of reinnervated PCs in the proximal zone of grafted cerebellar plates from explants of WT or Cry1$^{-/-}$Cry2$^{-/-}$ (DKO) embryos. In DKO explants, BHFS (n = 7) did not induce reinnervation compared with sham (n = 10) (one-way ANOVA with Tukey post hoc; P = 0.946), whereas BDNF (n = 7) did (P < 0.001). "WT BHFS" is given for comparison from Fig. 2.

responded to BDNF with significant reinnervation (Fig. 5). Thus, the cryptochrome-deficient olivocerebellar system is capable of developing reinnervating axon collaterals in response to BDNF. However, cryptochrome magnetoreceptors are required for LI-rMS–induced plasticity.

To clarify whether cryptochrome is involved in LI-rMS–induced climbing fiber reinnervation, we examined any potential link of its direct target, the *Clock/Arntl* transcriptional complex (*25*), to the expression of genes known to be involved in axon growth, plasticity, and/or regeneration. An in silico search of the 22 genes regulated by LI-rMS showed that eight (36%) contained CLOCK- or ARNTL-binding sequences in their upstream promoter regions (fig. S6), thus supporting cryptochrome involvement in LI-rMS–induced reinnervation.

DISCUSSION

We show that LI-rMS induced olivocerebellar reinnervation in vivo and ex vivo, similar to neurotrophin-induced repair (*17*, *18*). Reinnervation depended on the complex biomimetic patterns of stimulation, which up-regulated expression of growth-promoting genes. Reinnervation also required the presence of cryptochromes, adding a new mechanism through which low-intensity magnetic stimulation affects neural tissue: direct action of the magnetic field in addition to any subthreshold electric induction.

Reinnervation depends on magnetic stimulation pattern

This study is the first to demonstrate that specific biomimetic stimulation patterns are necessary for LI-rTMS (in vivo) and LI-rMS (ex vivo) to induce axonal outgrowth and reinnervation, even in a mature neural system (Figs. 1 and 2), similar to that induced by neurotrophic factors (*17*, *18*, *26*). In vivo climbing fiber–Purkinje cell reinnervation requires axonal outgrowth over several millimeters through a myelinated environment (*17*, *18*), enough to have direct relevance for human neural pathology and injury. This growth contrasts with previous studies on magnetic stimulation that have only demonstrated local changes to neurite terminals, synaptogenesis (*5*, *27*), or synapse elimination (*11*, *12*) and suggests that low-field magnetic stimulation has much greater potential for human treatment than previously reported.

We also show the importance of stimulation frequency and pattern on postlesion neural repair. Although human high-intensity rTMS stimulation frequencies are broadly divided into "excitatory" and "inhibitory," with iTBS and cTBS inducing the most consistent and long-lasting effects (*1*, *28*), our data greatly extend this concept. We show that complexity (iTBS is more effective than cTBS and 10 Hz) and regularity (iTBS is effective and R-iTBS is not) are more important than the number of pulses per se (iTBS has the same pulse number as R-iTBS, but much fewer than BHFS). iTBS and R-iTBS, which deliver the same number of pulses in slightly different patterns, thus providing an internal control for heat and/or vibration-induced artifacts (*20*), had contrasting effects: iTBS induced Purkinje cell reinnervation, whereas R-iTBS did not. These results demonstrate the critical importance of biologically relevant stimulation patterns, such as regular runs of theta activity, in the efficacy of magnetic stimulation (in this case, the production of neural circuit repair). In contrast, nonbiologically relevant magnetic fields disturb bird navigation (*29*) and are a potential public health concern (*30*). Therefore, greater understanding of the effects of different stimulation frequencies and patterns provides a basis for optimizing safe treatment protocols, which currently use standard (1 or >10 Hz) rTMS frequencies rather than TBS or other biomimetic patterns (*31*).

Although two studies have previously shown altered gene expression following magnetic stimulation (*10*, *32*), this report is the first demonstration that each stimulation pattern regulates the expression of specific genes, which are appropriate for the observed biological effect (producing neural circuit repair). For example, iTBS and BHFS each up-regulate the expression of 10 genes known to contribute to axon growth and neural plasticity, coherent with inducing the same biological outcome of reinnervation; but only 4 of these genes are common to both protocols (Fig. 4, table S3, and fig. S4), suggesting that the different stimulation patterns act through slightly different mechanisms. Among the functions of the gene products up-regulated by both of these effective stimulation patterns: β-Glucuronidase (*Gusb*) reduces extracellular matrix glycosaminoglycans to permit postlesion axon outgrowth (*16*); *B2m* promotes axon regeneration and selective synapse stabilization (*14*); and NT3 (*Ntf3*) enhances neural circuit repair through axon growth and synaptic plasticity in several pathways (*13*, *15*), including olivocerebellar climbing fibers (*17*, *33*). The *Gdnf* gene, whose product attracts axon growth cones (*34*), was down-regulated by R-iTBS, consistent with this pattern's failure to induce reinnervation. Our finding that different LI-rMS protocols can produce a common outcome (olivocerebellar reinnervation) by activating common core molecular pathways while retaining individual differences shows the potential for personalizing stimulation protocols according to the individual and/or specific disease, thus bringing NIBS into the field of personalized medicine.

The magnetic component of LI-rMS induces olivocerebellar reinnervation

A key discovery of our study is the requirement for the potential magnetoreceptor cryptochrome for LI-rMS–induced neural circuit repair. Stimulation of explants from cryptochrome DKOs did not produce climbing fiber–Purkinje cell reinnervation, although the successful reinnervation response to BDNF in these mutants confirmed

that cryptochrome is not needed for climbing fiber axonal outgrowth. This is the first direct evidence in the mouse central nervous system that mammalian cryptochromes are necessary for LI-rMS–induced axon growth and neosynaptogenesis.

Cryptochrome confers light-dependent magnetosensitivity in plants and insects (*23*, *24*, *35*, *36*) and light-independent functions such as magnetosensitivity in mammalian cells (*7*, *37*) and regulation of circadian rhythms (*22*, *38*, *39*). Cryptochromes are ubiquitously expressed flavoproteins that undergo conformational change and generate a radical pair in the presence of either light or, as in this study, magnetic fields (*25*, *40*). Radical pairs produce reactive oxygen species [ROS; (*40*)], and altered conformation removes cryptochrome inhibition of the *Clock/Arntl* transcriptional activity (*25*). Because ROS control many cellular processes (*41*) and CLOCK/ARNTL regulates numerous genes (*42*), cryptochrome has many cellular and molecular effects. An in silico search for CLOCK- or ARNTL-binding sequences revealed their presence in promoter regions of several of the genes whose expression was modulated by LI-rMS (fig. S6), thus supporting cryptochrome's role in mediating LI-rMS effects.

In addition, ROS generation within physiological concentrations could explain how LI-rMS increases the number of c-fos–positive cells (*20*, *35*), despite the induced electric field being below the action potential threshold (*21*). Both ROS (*43*) and LI-rMS (*10*) release calcium from intracellular stores, which, in turn, activates c-fos. Although LI-rMS induces c-fos in many cell types, its expression in denervated cells seems to play a role in their reinnervation. This hypothesis is supported by the fact that redox equilibrium is disturbed in denervated neurons (*44*), the pre-reinnervation status of our Purkinje cells and interneurons, which may account for the preferential c-fos activation in these two neuronal populations and thus their subsequent reinnervation. Moreover, in the groups where c-fos expression is not increased in the Purkinje and interneuron populations (sham, cTBS, and R-iTBS), LI-rMS does not induce climbing fiber–Purkinje cell reinnervation (Fig. 2).

These data suggest a new framework for understanding the neurobiological effects of low-intensity magnetic stimulation. Because low-intensity magnetic fields do not directly trigger neuronal firing, we argue that the magnetic field itself, acting, at least in part, through cryptochromes, activates a broad range of cellular events. This demonstration of direct action of the magnetic field requires a shift from current thinking, in which magnetic induction of electric currents acts by altering neuronal firing to induce neuroplasticity. This new framework must include the effects of the magnetic field on cellular function in addition to any effect generated by the weak, nondepolarizing electric field. This framework not only explains clinical (*3*, *4*) and experimental (*7*–*10*) findings but also provides biological mechanisms that open the potential to develop specific LI-rTMS programs for individual neurological conditions.

CONCLUSION

LI-rTMS induces axon outgrowth and targeted neosynaptogenesis in olivocerebellar reinnervation, both in vivo and ex vivo. This reinnervation depends on cryptochrome magnetoreceptors and biologically relevant stimulation patterns. Our data suggest that LI-rTMS acts on cryptochrome to trigger intracellular signaling, including changes in gene expression, that contributes to neural repair. Because cryptochrome activation can act on many intracellular targets, our findings point to the possibility of developing LI-rTMS protocols that target a range of biological questions and clinical challenges.

MATERIALS AND METHODS

Study design

Research objectives and experimental design

This controlled laboratory study aimed to test the hypothesis that low-intensity magnetic stimulation (LI-rTMS) can produce post-lesion repair in the olivocerebellar path and to identify the underlying mechanisms. Mechanisms studied were stimulation parameters, gene expression changes, and the involvement of the magnetic field through cryptochrome magnetoreceptor.

We first took 3-month-old adult male mice with a unilateral olivocerebellar lesion and randomly allocated them for treatment with BHFS LI-rTMS or sham (10 min/day for 2 weeks) before perfusion and histological evaluation of reinnervation. To identify optimal stimulation parameters, we chose our ex vivo organotypic model of the olivocerebellar path (*45*) and its reinnervation (lesioned, cocultured explants). Cocultured explants were treated (10 min/day for 2 weeks) with one from a range of LI-rTMS protocols (1 Hz, 10 Hz, cTBS, iTBS, R-iTBS, or BHFS) or sham stimulation. Twenty-four hours after the last stimulation, explants were fixed and treated for histological quantitation of reinnervation.

To examine the mechanisms underlying LI-rTMS–induced reinnervation, cocultured explants were stimulated (i) once to observe cellular activation, shown by c-fos expression, or (ii) with three daily sessions for subsequent gene expression during the time of reinnervation. These tests were made for BHFS and iTBS, two stimulation patterns inducing robust reinnervation, and R-iTBS with the same pulse number as iTBS but without inducing reinnervation. cTBS, which is an inhibitory stimulation pattern, was also tested for c-fos expression only. In addition, to test the role of the magnetic field in reinnervation, explants from cryptochrome DKO mice were stimulated with BHFS for 2 weeks before histological analysis of reinnervation. Confirmation of the effects of different LI-rTMS patterns and the involvement of Cry was not repeated in vivo because these experiments would not provide additional information about underlying mechanisms and the large increase in animal surgery is not compatible with the European Communities Council Directive 2010/63/EU on animal experimentation.

Sample size

Sample size was determined on the basis of our previous experience with the lesion model in vivo; in general, five or more individuals per experimental group were used.

Data inclusion/exclusion criteria

For the in vivo experiments, individuals were included only if the peduncolotomy lesion was complete, as determined by histological analysis at the time of quantification of reinnervation (*17*, *18*). For the ex vivo experiments, explants showing abnormal morphology were excluded. This represented less than 1% of explants.

Outliers

Potential outliers were identified in SPSS, using the ROUT method with Q set to 1% (i.e., less than 1% of detected outliers would be in error). In the studies reported here, no data were discarded.

Replicates

The quantitative reverse transcription polymerase chain reaction (qRT-PCR) data were obtained from RT^2 Profiler PCR Array Mouse

Neurotrophins and Receptors plates (QIAGEN), on which there were three replicates of each sample. The mean of these three was used in the subsequent analysis. To obtain each sample, RNA was obtained from pooled tissue of six cerebellar plates (three embryonic explants), and there were five independent samples for each stimulation group.

Randomization

Pedunculotomized mice were randomly allocated to either sham or LI-rTMS groups. For the ex vivo explants, dissected embryos from a litter were randomly allocated to different stimulation groups, such that all groups contained explants from at least three litters, and each litter contributed to several groups.

Blinding

Histological evaluation of reinnervation, for both the in vivo and explant experiments, was carried out blind to the treatment group of the sample being evaluated. In some experimental groups, more than one experimenter measured reinnervation; in those cases, we verified that the results did not differ by more than 5% between experimenters.

Animals

Animal housing and all procedures were authorized either by the Comité National d'Ethique pour les Sciences de la Vie et de la Santé (no. 1492-02) or the University of Western Australia Animal Ethics Committee (no. 03/100/834), in accordance with the European Communities Council Directive 2010/63/EU and the regulations of the National Health and Medical Research Council of Australia and the NIH. Three-month-old adult male inbred C57Bl/6j mice were purchased from the Animal Resources Centre (Murdoch, Western Australia) and timed pregnant Swiss mice from Janvier Labs (Villejuif, France). Cryptochrome DKO ($Cry1^{-/-}Cry2^{-/-}$) mice were a gift from X.-M. Li and F. Lévi. $Cry1^{-/-}Cry2^{-/-}$ embryos were obtained from timed mating between $Cry1^{-/-}Cry2^{-/-}$ male mice and $Cry1^{-/-}Cry2^{+/-}$ female mice. The mouse phenotype has been described previously (*22*) and did not reveal any abnormalities of motor function that would suggest cerebellar dysfunction. For completeness, we described the potential links of Cry to cerebellar development in the Supplementary Materials (fig. S3).

Genotyping

Briefly, tissue was digested overnight at 55°C with proteinase K (QIAGEN, France) in TSE buffer containing 25 mM tris-HCl (pH 8.0), 75 mM NaCl, 25 mM EDTA (pH 8.0), and 1% SDS (Sigma-Aldrich, France). DNA fragments were precipitated with isopropanol and washed with 70% ethanol before being dissolved in 100 µl of distilled water. DNA was amplified by PCR, and the amplified fragments were detected by electrophoresis on a 2% agarose gel. The following primers were used: Cry1 P1 (WT) Ex5, 5′-TGAGGCACTTACACGTTTGG-3′; Cry1 P2 (KO), 5′-TGAATGAACTGCAGGACGAG-3′; Cry1 P3 (WT/KO), 5′-ATCCCTTCTTCCCAGCTGAT-3′; Cry2 P1 (WT), 5′-CCAGAGACGGGAAATGTTCTT-3′; Cry2 P2 (KO), 5′-GAGATCAGCAGCCTCTGTTCC-3′; Cry2 P3 (WT/KO), 5′-GCTTCATCCACATCGGTAACTC-3′.

In vivo olivocerebellar axonal transection (pedunculotomy)

Our repair readout is the postlesion restoration of climbing fibers, which connect the ION to Purkinje cells of the cerebellum (*17*–*19*). Unilateral climbing fiber transection removes all climbing fibers from a hemicerebellum and leads to degeneration of the axotomized inferior olive. Intracerebellar injection of neurotrophic factors can induce neurons of the remaining inferior olive to develop transcommissural axon collaterals that cross the cerebellar midline and partially reinnervate the denervated hemicerebellum and compensate motor coordination and spatial learning behaviors (*18*).

WT mice were anesthetized with xylazine [10 mg/kg, intraperitoneally (ip)] and ketamine (70 mg/kg, ip; Ilium, New South Wales, Australia) and underwent unilateral transection of the left inferior cerebellar peduncle, as previously described (*17*, *18*). Briefly, the skin over the neck was incised longitudinally, and the muscles retracted to expose the atlanto-occipital membrane. A capsulotomy knife (3-mm blade; MSP) was inserted parallel to the brainstem into the fourth ventricle and rotated to the left to cut the left inferior cerebellar peduncle. After recovery from the anesthetic, animals were returned to the cage. Food and water were provided ad libitum.

Organotypic cultures and cerebellar denervation

The olivocerebellar pathway can also be studied ex vivo using organotypic hindbrain explants that contain the whole circuit, are highly reproducible, and are readily manipulated (*45*), so that we can reproduce the pedunculotomy lesion. These explants have been extensively characterized: They develop all cerebellar neuronal populations and normal cerebellar cortical circuitry so that Purkinje cells receive normal spontaneous input from their parallel and climbing fiber afferents (*45*).

Hindbrain explants were cultured from embryonic Swiss or cryptochrome DKO ($Cry1^{-/-}Cry2^{-/-}$) mice at embryonic day 14 (E14), as previously described (*45*). E0 was the mating day. Following anesthesia and cervical dislocation of pregnant female mice, embryos were removed, and their brains were quickly dissected in ice-cold Gey's balanced salt solution (Eurobio) containing glucose (5 mg/ml). The hindbrain, including the cerebellar anlage and ION, was isolated, and the meninges were removed. The right and left cerebellar plates were separated at the midline (fig. S1), and the explants were transferred onto 30-mm Millicell membranes (pore size, 0.4 µm; Millipore) and then cultured with medium, containing 50% basal medium with Earle's salts (Gibco), 2.5% Hanks' balanced salt solution (Gibco), 25% horse serum (Gibco), 1 mM L-glutamine (Gibco), and glucose (5 mg/ml), at 35°C in humidified air with 5% CO_2. The culture day was designated 0 day in vitro (DIV). The medium was replaced every 2 to 3 days. For each litter, embryos were randomly assigned to different treatment groups, so that each treatment protocol group contained explants from at least three litters and each litter of embryos contributed to several experimental groups.

To denervate cerebellar tissue and induce olivocerebellar reinnervation, we removed the cerebellar plates from their explant brainstem at 21 DIV [equivalent to postnatal day 15 (P15)] and cocultured them (graft) adjacent to the cerebellar plate of an intact explant (host; fig. S1). This effectively reproduces the in vivo lesion in which, in the presence of trophic factors, undamaged climbing fibers from the intact host cerebellum sprout axon collaterals that enter the graft and pass the deep nuclei to reach denervated Purkinje cells in the outer cortical layers.

Magnetic stimulation

The in vivo mouse cerebellum and the in vitro hindbrain cerebellar explants are different sizes and shapes. Thus, to give them equivalent magnetic stimulation, we used different stimulation coils that were an appropriate size for the different tissues.

In vivo

Pedunculotomized mice recovered for 3 days after surgery before being randomly allocated to groups receiving LI-rTMS or sham treatment (10 min/day for 14 consecutive days), as previously described (*11*, *12*). An electromagnetic pulse generator (EC10701, Global Energy Medicine, Perth, Australia) was modified for the attachment of a custom-designed copper wire (0.25-mm diameter, 16 ohms; Jaycar) coil with an outer diameter of 8 mm, 300 windings, and a 6-mm-diameter steel bolt in the center to increase field penetration into the brain (*11*). The nonsinusoidal monophasic 300-μs pulse had a measured 230-μs rise time, in which the steel bolt had prolonged from its theoretical 100-μs value, and generated a magnetic field intensity of 8 to 10 mT at the distance of the cerebellar cortex, without sound, vibration, or heat above background (*12*). The coil size was designed to ensure a similar coil-to-brain ratio as used for focal magnetic stimulation in humans (*46*).

Ex vivo

To investigate which parameters were most effective for inducing reinnervation, pedunculotomized explants received LI-rMS (identical to LI-rTMS, but not transcranial) inside the incubator (10 min/day for 14 days) using a custom-built copper wire coil (wire thickness, 0.4 mm; coil, 10-mm inside diameter; 26-mm outside diameter; 199 turns) placed 4 mm below the well and driven by a 24-V magnetic pulse generator (*20*). The nonsinusoidal monophasic 300-μs pulse had a measured 100-μs rise time and generated a magnetic intensity of 10 mT and electric fields of 0.05 to 0.075 V/m at the distance of the explant (4 mm), without vibration or heating above background (*20*). Each culture plate was isolated from others using mu-metal (nickel/iron/molybdenum alloy) shielding to ensure no eddy current spill over. In some experiments, mu-metal was used to shield either the rostral or caudal part of the explant from the stimulation.

We chose stimulation patterns (fig. S1) that were used in human clinical rTMS: simple pulse stimulation at 1 and 10 Hz; complex frequencies with a TBS pattern (three-pulse bursts at 50 Hz repeated at 5 Hz), delivered continuously (cTBS), intermittently (iTBS) for 2 s repeated every 10 s, or randomly (R-iTBS; three-pulse bursts at 50 Hz repeated randomly at 2 to 60 Hz, for 2 s, all repeated every 10 s). We also tested a complex BHFS, which, we have previously shown, can modulate neural circuits (*11*, *12*). Sham treatment was delivered identically but without activation of the stimulation coil.

Immunohistochemistry

Pedunculotomized mice were euthanized 24 hours after the last stimulation (18 days after lesion) with an overdose of sodium pentothal and perfused transcardially with 0.9% saline and 4% paraformaldehyde in 0.1 M phosphate buffer. The brain was postfixed in fresh 4% paraformaldehyde overnight at 4°C and cryoprotected in 30% sucrose, and coronal cryosections of the cerebellum and brainstem were cut at 20 μm. For ex vivo experiments, 24 hours after the last stimulation session, explants were fixed with 4% paraformaldehyde for 4 hours at 4°C.

Sections and explants were labeled by immunohistochemistry. Fixed tissue was rinsed three times for 5 min in phosphate-buffered saline containing 0.25% Triton X-100 (PBS-T) and blocked in 20% donkey serum for 2 hours at room temperature before incubation overnight at 4°C in primary antibody diluted in PBS-TG [PBS-T containing 0.2% gelatin and L-lysine (0.018 g/ml)]. The next day, sections or explants were washed three times for 5 min in PBS-T, and labeling was visualized with fluorescent-conjugated secondary antibodies in PBS-TG for 2 hours at room temperature. Last, sections or explants were rinsed and mounted in Mowiol.

To identify climbing fiber reinnervation, Purkinje cells were labeled with rabbit anti–calbindin-D-28K (CB) antibody (1:3000; Swant), and climbing fiber terminals were labeled with polyclonal guinea pig anti-VGLUT2 antibody (1:2000; Millipore) (*17*, *18*, *45*). Primary antibodies were visualized using Cy3-conjugated donkey anti–guinea pig and Alexa Fluor 488 (AF488)–conjugated donkey anti-rabbit (1:200 and 1:400, respectively; the Jackson laboratory).

To identify which cells were activated by the magnetic stimulation ex vivo, we labeled for c-fos 2.5 hours after a single 10-min stimulation session 72 hours after lesion and coculture. Fixed explants were labeled with rabbit anti–c-fos (1:3000; Synaptic Systems) and one of four different antibodies to identify specific cell populations (*47*): Purkinje cells with monoclonal mouse anti-CB (1:2000; Swant), GABAergic interneurons with goat anti-parvalbumin (1:3000; Swant), and granule cells with monoclonal mouse anti-NeuN (1:200; Millipore). Primary antibody binding was visualized using Cy3-conjugated donkey anti-rabbit, AF488-conjugated donkey anti-goat, and Cy5-conjugated donkey anti-mouse (all 1:200; the Jackson laboratory).

Histological analysis

Quantification of olivocerebellar reinnervation

In in vivo experiments, cerebellum-brainstem sections were analyzed to verify the completeness of the pedunculotomy lesion according to established criteria: (i) total degeneration of the right inferior olive, (ii) separation of the left hemicerebellum from the brainstem at the level of the inferior cerebellar peduncle, and (iii) residual left deep cerebellar nuclei (*17*, *18*). If any of these criteria were not verified or if other damage was present to the brainstem or ventral cerebellum, the animal was excluded from analysis.

To quantify the extent of reinnervation, the cerebellum of pedunculotomized animals was divided into a series of parasagittal zones (500 μm wide) extending from the midline to the left lateral hemicerebellum. Within each zone, the amount of VGLUT2-positive climbing fiber reinnervation was scored in each lobule using an arbitrary scale, i.e., 1 = few strands; 2 = one-quarter climbing fiber-filled lobule; 3 = half lobule; 4 = three-quarter lobule; and 5 = completely climbing fiber-filled lobule. Scores in each 500-μm zone of each lobule are the mean values from all animals and are plotted on an unfolded cerebellar cortex to give a semiquantitative evaluation of climbing fiber reinnervation, as described previously (*18*).

In ex vivo experiments, labeled explants were examined using epifluorescence microscopy (DM 6000F, Leica), and *z*-stack images were taken for analysis. Climbing fiber reinnervation was quantified by counting the number of CB-positive Purkinje cells (soma and primary dendrites) colocalized with VGLUT2 per field of view and expressed as the percentage of Purkinje cells per field. To ensure that the stimulation did not significantly alter CB expression, which could have resulted in either weakly labeled cells being missed or very strongly labeled cells hiding the VGLUT2, we verified that there was a similar number of CB-positive Purkinje cells visible per hemicerebellum (table S1). In addition, the climbing fiber quantification was made on *z*-stacks, hiding each color channel as necessary to ensure that VGLUT2 puncta were not missed. *z*-stacks were taken systematically in rows through the cerebellar graft with increasing distance from the host-graft interface (fig. S1). Data from rows 1 and 2 were defined as the proximal zone, and those from rows 3 to 5 were defined as the distal zone.

Cellular activation: c-fos

Explants were examined using epifluorescence microscopy, and *z*-stack images were taken at three systematic randomly selected sites of 0.073 mm^2 for each cocultured cerebellar plate. Total c-fos–positive staining was counted per *z*-stack, and double- or triple-labeled profiles were examined for colabeling. c-fos–, CB-, and PV-positive cells were counted per image to identify the proportions activated by LI-rMS. To ensure that our data were representative, we counted a minimum of 450 Purkinje cells and 250 interneurons per group as numbers varied between the individual images (table S2). Results were expressed as mean number of c-fos–positive cells per square millimeter.

Quantitative reverse transcription polymerase chain reaction

Changes in gene expression, triggered by different LI-rMS frequencies, were examined in a separate series of explants following effective and ineffective reinnervation protocols. Explants were denervated and cocultured at 21 DIV (P15), and 72 hours after the lesion, they received three daily sessions (10 min/day) of LI-rMS/sham. The cerebellar plate of denervated treated explants was taken 6 hours after the last stimulation (P18). For each sample, six cerebellar plates were pooled, and total RNA was extracted using TRIzol (Life Technologies) according to the manufacturer's instructions and stored at −80°C.

Complementary DNA (cDNA) was transcribed from 400 ng of total RNA using the RT^2 Easy First Strand cDNA Synthesis Kit (QIAGEN). For each sample, the resulting cDNA was applied to the RT^2 Profiler PCR Array Mouse Neurotrophins and Receptors (QIAGEN; table S4) and amplified with a LightCycler 480 System. Results were analyzed on the QIAGEN RT^2 Profiler PCR array data analysis (v3.5) using the housekeeping gene, hsp90ab1. Normalized mean expression levels ($\log_2^{-\Delta\Delta Ct}$) were used to determine differentially expressed genes between each group and control.

Statistical analysis

All data were explored for normality, outliers, and fulfillment of statistical test assumptions in SPSS 22 (IBM Corp., Armonk, NY). Reinnervation scores were analyzed with repeated-measures ANOVA (*F*) (location × stimulation). When significant interaction between stimulation and location was present, univariate ANOVA was performed to evaluate the effect of the treatment in proximal and distal zones independently. Tukey post hoc comparisons were performed where appropriate. c-fos activation by different LI-rMS protocols was analyzed with univariate ANOVA and Tukey post hoc comparisons. Percentages of CB- and PV-positive labeled neurons, which were also c-fos positive (CB/c-fos, PV/c-fos), were analyzed with χ^2, and since we only wanted to compare differences from sham stimulation, we used the 2 × 2 variant, Fisher's exact test. Gene expression levels were compared by two-sample *t* test. All values are expressed as means ± SEM and considered significant at $P < 0.05$. For ease of reading the manuscript, statistics are presented in the figure legends rather than the main text.

The function and linkage of regulated genes were examined for GO term enrichment using the R topGO package. Searching for GO biological process, molecular function, or cellular component (GO.db 3.3), each list of genes was analyzed by the topGO overrepresentation test against the *Mus musculus* reference list. The Bonferroni correction for multiple testing was applied. Using R (3.3.0) and the Bioconductor suite (3.3), we applied Biostrings (2.40) and the GenomicFeatures (1.24) to determine potential transcription factor binding sequences in our regulated genes. Transcription factor binding matrices [position weight matrix (PWM)] were obtained from the R package MotifDb (1.14) and compared, using matchPWM (with position at 90%), to target sequences in the promoter site and for 2-kb upstream.

SUPPLEMENTARY MATERIALS

Supplementary material for this article is available at http://advances.sciencemag.org/cgi/content/full/5/10/eaav9847/DC1

Fig. S1. Experimental protocol for LI-rMS to an ex vivo model of the olivocerebellar path.
Fig. S2. Distribution of c-fos in the graft and host cerebellum after LI-rMS.
Fig. S3. Relation of cryptochrome to cerebellar development.
Fig. S4. Specific LI-rMS patterns modulate gene expression appropriately for PC reinnervation.
Fig. S5. Relationships between genes regulated by different LI-rMS patterns.
Fig. S6. Genes regulated by different LI-rMS patterns contain binding sites for the transcription factors CLOCK and ARNTL1.
Table S1. Average number of Purkinje cells per cerebellar plate following 14 days of LI-rMS.
Table S2. Average numbers of cells counted per cerebellar plate labeled for c-fos.
Table S3. Biological pathways of genes regulated by LI-rMS.
Table S4. Genes examined on the RT^2 Profiler PCR Array Mouse Neurotrophins and Receptors.
References (*48*–*54*)

View/request a protocol for this paper from *Bio-protocol*.

REFERENCES AND NOTES

1. G. S. Pell, Y. Roth, A. Zangen, Modulation of cortical excitability induced by repetitive transcranial magnetic stimulation: Influence of timing and geometrical parameters and underlying mechanisms. *Prog. Neurobiol.* **93**, 59–98 (2011).
2. P. M. Rossini, D. Burke, R. Chen, L. G. Cohen, Z. Daskalakis, R. Di Iorio, V. Di Lazzaro, F. Ferreri, P. B. Fitzgerald, M. S. George, M. Hallett, J. P. Lefaucheur, B. Langguth, H. Matsumoto, C. Miniussi, M. A. Nitsche, A. Pascual-Leone, W. Paulus, S. Rossi, J. C. Rothwell, H. R. Siebner, Y. Ugawa, V. Walsh, U. Ziemann, Non-invasive electrical and magnetic stimulation of the brain, spinal cord, roots and peripheral nerves: Basic principles and procedures for routine clinical and research application. An updated report from an I.F.C.N. Committee. *Clin. Neurophysiol.* **126**, 1071–1107 (2015).
3. V. Di Lazzaro, F. Capone, F. Apollonio, P. A. Borea, R. Cadossi, L. Fassina, C. Grassi, M. Liberti, A. Paffi, M. Parazzini, K. Varani, P. Ravazzani, A consensus panel review of central nervous system effects of the exposure to low-intensity extremely low-frequency magnetic fields. *Brain Stimul.* **6**, 469–476 (2013).
4. M. L. Rohan, R. T. Yamamoto, C. T. Ravichandran, K. R. Cayetano, O. G. Morales, D. P. Olson, G. Vitaliano, S. M. Paul, B. M. Cohen, Rapid mood-elevating effects of low field magnetic stimulation in depression. *Biol. Psychiatry* **76**, 186–193 (2014).
5. M. S. Markov, Expanding use of pulsed electromagnetic field therapies. *Electromagn. Biol. Med.* **26**, 257–274 (2007).
6. I. Gunay, T. Mert, Pulsed magnetic fields enhance the rate of recovery of damaged nerve excitability. *Bioelectromagnetics* **32**, 200–208 (2011).
7. S. Di Loreto, S. Falone, V. Caracciolo, P. Sebastiani, A. D'Alessandro, A. Mirabilio, V. Zimmitti, F. Amicarelli, Fifty hertz extremely low-frequency magnetic field exposure elicits redox and trophic response in rat-cortical neurons. *J. Cell. Physiol.* **219**, 334–343 (2009).
8. Y. Yang, L. Li, Y.-G. Wang, Z. Fei, J. Zhong, L.-Z. Wei, Q.-F. Long, W.-P. Liu, Acute neuroprotective effects of extremely low-frequency electromagnetic fields after traumatic brain injury in rats. *Neurosci. Lett.* **516**, 15–20 (2012).
9. R. Piacentini, C. Ripoli, D. Mezzogori, G. B. Azzena, C. Grassi, Extremely low-frequency electromagnetic fields promote in vitro neurogenesis via upregulation of Ca_v1-channel activity. *J. Cell. Physiol.* **215**, 129–139 (2008).
10. S. Grehl, H. M. Viola, P. I. Fuller-Carter, K. W. Carter, S. A. Dunlop, L. C. Hool, R. M. Sherrard, J. Rodger, Cellular and molecular changes to cortical neurons following low intensity repetitive magnetic stimulation at different frequencies. *Brain Stimul.* **8**, 114–123 (2015).
11. K. Makowiecki, A. R. Harvey, R. M. Sherrard, J. Rodger, Low-intensity repetitive transcranial magnetic stimulation improves abnormal visual cortical circuit topography and upregulates BDNF in mice. *J. Neurosci.* **34**, 10780–10792 (2014).
12. J. Rodger, C. Mo, T. Wilks, S. A. Dunlop, R. M. Sherrard, Transcranial pulsed magnetic field stimulation facilitates reorganization of abnormal neural circuits and corrects behavioral deficits without disrupting normal connectivity. *FASEB J.* **26**, 1593–1606 (2012).
13. H.-H. Chen, W. G. Tourtellotte, E. Frank, Muscle spindle-derived neurotrophin 3 regulates synaptic connectivity between muscle sensory and motor neurons. *J. Neurosci.* **22**, 3512–3519 (2002).
14. A. L. R. Oliveira, S. Thams, O. Lidman, F. Piehl, T. Hökfelt, K. Kärre, H. Lindå, S. Cullheim, A role for MHC class I molecules in synaptic plasticity and regeneration of neurons after axotomy. *Proc. Natl. Acad. Sci. U.S.A.* **101**, 17843–17848 (2004).

15. L. Schnell, R. Schneider, R. Kolbeck, Y. A. Barde, M. E. Schwab, Neurotrophin-3 enhances sprouting of corticospinal tract during development and after adult spinal cord lesion. *Nature* **367**, 170–173 (1994).
16. P. D. Smith, V. J. Coulson-Thomas, S. Foscarin, J. C. F. Kwok, J. W. Fawcett, "GAG-ing with the neuron": The role of glycosaminoglycan patterning in the central nervous system. *Exp. Neurol.* **274**, 100–114 (2015).
17. R. M. Sherrard, A. J. Bower, BDNF and NT3 extend the critical period for developmental climbing fibre plasticity. *Neuroreport* **12**, 2871–2874 (2001).
18. M. L. Willson, C. McElnea, J. Mariani, A. M. Lohof, R. M. Sherrard, BDNF increases homotypic olivocerebellar reinnervation and associated fine motor and cognitive skill. *Brain* **131**, 1099–1112 (2008).
19. I. Sugihara, Y. Shinoda, Molecular, topographic, and functional organization of the cerebellar cortex: A study with combined aldolase C and olivocerebellar labeling. *J. Neurosci.* **24**, 8771–8785 (2004).
20. S. Grehl, D. Martina, C. Goyenvalle, Z.-D. Deng, J. Rodger, R. M. Sherrard, In vitro magnetic stimulation: A simple stimulation device to deliver defined low intensity electromagnetic fields. *Front. Neural Circuits* **10**, 85 (2016).
21. C. Y. Chan, C. Nicholson, Modulation by applied electric fields of Purkinje and stellate cell activity in the isolated turtle cerebellum. *J. Physiol.* **371**, 89–114 (1986).
22. G. T. van der Horst, M. Muijtjens, K. Kobayashi, R. Takano, S. Kanno, M. Takao, J. de Wit, A. Verkerk, A. P. Eker, D. van Leenen, R. Buijs, D. Bootsma, J. H. Hoeijmakers, A. Yasui, Mammalian Cry1 and Cry2 are essential for maintenance of circadian rhythms. *Nature* **398**, 627–630 (1999).
23. T. Yoshii, M. Ahmad, C. Helfrich-Förster, Cryptochrome mediates light-dependent magnetosensitivity of *Drosophila's* circadian clock. *PLOS Biol.* **7**, e1000086 (2009).
24. R. Marley, C. N. G. Giachello, N. S. Scrutton, R. A. Baines, A. R. Jones, Cryptochrome-dependent magnetic field effect on seizure response in Drosophila larvae. *Sci. Rep.* **4**, 5799 (2014).
25. C. Lin, T. Todo, The cryptochromes. *Genome Biol.* **6**, 220 (2005).
26. R. Vavrek, J. Girgis, W. Tetzlaff, G. W. Hiebert, K. Fouad, BDNF promotes connections of corticospinal neurons onto spared descending interneurons in spinal cord injured rats. *Brain* **129**, 1534–1545 (2006).
27. J. Ma, Z. Zhang, Y. Su, L. Kang, D. Geng, Y. Wang, F. Luan, M. Wang, H. Cui, Magnetic stimulation modulates structural synaptic plasticity and regulates BDNF-TrkB signal pathway in cultured hippocampal neurons. *Neurochem. Int.* **62**, 84–91 (2013).
28. Y.-Z. Huang, M. J. Edwards, E. Rounis, K. P. Bhatia, J. C. Rothwell, Theta burst stimulation of the human motor cortex. *Neuron* **45**, 201–206 (2005).
29. R. Wiltschko, W. Wiltschko, Sensing magnetic directions in birds: Radical pair processes involving cryptochrome. *Biosensors* **4**, 221–242 (2014).
30. I. Belyaev, A. Dean, H. Eger, G. Hubmann, R. Jandrisovits, M. Kern, M. Kundi, H. Moshammer, P. Lercher, K. Müller, G. Oberfeld, P. Ohnsorge, P. Pelzmann, C. Scheingraber, R. Thill, EUROPAEM EMF Guideline 2016 for the prevention, diagnosis and treatment of EMF-related health problems and illnesses. *Rev. Environ. Health* **31**, 363–397 (2016).
31. A. R. Brunoni, A. Chaimani, A. H. Moffa, L. B. Razza, W. F. Gattaz, Z. J. Daskalakis, A. F. Carvalho, Repetitive transcranial magnetic stimulation for the acute treatment of major depressive episodes: A systematic review with network meta-analysis. *JAMA Psychiat.* **74**, 143–152 (2017).
32. L. X. Wei, R. Goodman, A. Henderson, Changes in levels of c-myc and histone H2B following exposure of cells to low-frequency sinusoidal electromagnetic fields: Evidence for a window effect. *Bioelectromagnetics* **11**, 269–272 (1990).
33. I. Neveu, E. Arenas, Neurotrophins promote the survival and development of neurons in the cerebellum of hypothyroid rats in vivo. *J. Cell Biol.* **133**, 631–646 (1996).
34. U. Drescher, Axon guidance: Push and pull with ephrins and GDNF. *Curr. Biol.* **21**, R30–R32 (2011).
35. G. Fedele, M. D. Edwards, S. Bhutani, J. M. Hares, M. Murbach, E. W. Green, S. Dissel, M. H. Hastings, E. Rosato, C. P. Kyriacou, Genetic analysis of circadian responses to low frequency electromagnetic fields in *Drosophila melanogaster*. *PLOS Genet.* **10**, e1004804 (2014).
36. G. Fedele, E. W. Green, E. Rosato, C. P. Kyriacou, An electromagnetic field disrupts negative geotaxis in *Drosophila* via a CRY-dependent pathway. *Nat. Commun.* **5**, 4391 (2014).
37. R. M. Sherrard, N. Morellini, N. Jourdan, M. El-Esawi, L.-D. Arthaut, C. Niessner, F. Rouyer, A. Klarsfeld, M. Doulazmi, J. Witczak, A. d'Harlingue, J. Mariani, I. Mclure, C. F. Martino, M. Ahmad, Low-intensity electromagnetic fields induce human cryptochrome to modulate intracellular reactive oxygen species. *PLoS Biol.* **16**, e2006229 (2018).
38. R. J. Kutta, N. Archipowa, L. O. Johannissen, A. R. Jones, N. S. Scrutton, Vertebrate cryptochromes are vestigial flavoproteins. *Sci. Rep.* **7**, 44906 (2017).
39. C. A. Dodson, P. J. Hore, M. I. Wallace, A radical sense of direction: Signalling and mechanism in cryptochrome magnetoreception. *Trends Biochem. Sci.* **38**, 435–446 (2013).
40. L.-D. Arthaut, N. Jourdan, A. Mteyrek, M. Procopio, M. El-Esawi, A. d'Harlingue, P.-E. Bouchet, J. Witczak, T. Ritz, A. Klarsfeld, S. Birman, R. J. Usselman, U. Hoecker, C. F. Martino, M. Ahmad, Blue-light induced accumulation of reactive oxygen species is a consequence of the Drosophila cryptochrome photocycle. *PLOS ONE* **12**, e0171836 (2017).
41. P. D. Ray, B.-W. Huang, Y. Tsuji, Reactive oxygen species (ROS) homeostasis and redox regulation in cellular signaling. *Cell. Signal.* **24**, 981–990 (2012).
42. F. Hatanaka, C. Matsubara, J. Myung, T. Yoritaka, N. Kamimura, S. Tsutsumi, A. Kanai, Y. Suzuki, P. Sassone-Corsi, H. Aburatani, S. Sugano, T. Takumi, Genome-wide profiling of the core clock protein BMAL1 targets reveals a strict relationship with metabolism. *Mol. Cell. Biol.* **30**, 5636–5648 (2010).
43. A. Görlach, K. Bertram, S. Hudecova, O. Krizanova, Calcium and ROS: A mutual interplay. *Redox Biol.* **6**, 260–271 (2015).
44. O. M. E. Abdel-Salam, R. F. Abdel-Rahman, A. A. Sleem, F. A. Mosry, H. A. Sharaf, Effects of afferent and efferent denervation of vagal nerve on endotoxin-induced oxidative stress in rats. *J. Neural Transm.* **120**, 1673–1688 (2013).
45. M. Letellier, R. Wehrlé, J. Mariani, A. M. Lohof, Synapse elimination in olivo-cerebellar explants occurs during a critical period and leaves an indelible trace in Purkinje cells. *Proc. Natl. Acad. Sci. U.S.A.* **106**, (2009), doi:10.1073/pnas.0902820106.
46. J. D. Weissman, C. M. Epstein, K. R. Davey, Magnetic brain stimulation and brain size: Relevance to animal studies. *Electroencephalogr. Clin. Neurophysiol.* **85**, 215–219 (1992).
47. A. Weyer, K. Schilling, Developmental and cell type-specific expression of the neuronal marker NeuN in the murine cerebellum. *J. Neurosci. Res.* **73**, 400–409 (2003).
48. S. N. Anand, E. S. Maywood, J. E. Chesham, G. Joynson, G. T. Banks, M. H. Hastings, P. M. Nolan, Distinct and separable roles for endogenous CRY1 and CRY2 within the circadian molecular clockwork of the suprachiasmatic nucleus, as revealed by the Fbxl3Afh mutation. *J. Neurosci.* **33**, 7145–7153 (2013).
49. D. De Bundel, G. Gangarossa, A. Biever, X. Bonnefont, E. Valjent, Cognitive dysfunction, elevated anxiety, and reduced cocaine response in circadian clock-deficient cryptochrome knockout mice. *Front. Behav. Neurosci.* **7** (2013), doi:10.3389/fnbeh.2013.00152.
50. G. Griebel, C. Ravinet-Trillou, S. Beeské, P. Avenet, P. Pichat, Mice deficient in cryptochrome 1 ($Cry1^{-/-}$) exhibit resistance to obesity induced by a high-fat diet. *Front. Endocrinol.* **5**, 49 (2014).
51. G.-J. Huang, A. Edwards, C.-Y. Tsai, Y.-S. Lee, L. Peng, T. Era, Y. Hirabayashi, C.-Y. Tsai, S.-I. Nishikawa, Y. Iwakura, S.-J. Chen, J. Flint, Ectopic cerebellar cell migration causes maldevelopment of Purkinje cells and abnormal motor behaviour in Cxcr4 null mice. *PLOS ONE* **9**, e86471 (2014).
52. M. Luz, E. Mohr, H. C. Fibiger, GDNF-induced cerebellar toxicity: A brief review. *Neurotoxicology* **52**, 46–56 (2016).
53. W. Lin, A. Kemper, K. D. McCarthy, P. Pytel, J.-P. Wang, I. L. Campbell, M. F. Utset, B. Popko, Interferon-gamma induced medulloblastoma in the developing cerebellum. *J. Neurosci.* **24**, 10074–10083 (2004).
54. J. Wang, W. Lin, B. Popko, I. L. Campbell, Inducible production of interferon-gamma in the developing brain causes cerebellar dysplasia with activation of the Sonic hedgehog pathway. *Mol. Cell. Neurosci.* **27**, 489–496 (2004).

Acknowledgments: We thank A. Tobin for helpful comments on the manuscript. **Funding:** This work was supported by the Institut pour la Recherche sur la Moelle Epinière et l'Encéphale, the CNRS, and the Paris region Ile de France (CPER). T.D. and S.G. had PhD scholarships from the French Ministry of Education and the University of Western Australia, respectively. Z.-D.D. was supported by the National Institute of Mental Health Intramural Research Program, NIH. **Author contributions:** R.M.S. and T.D. designed the experiments. T.D., S.G., A.D.T., and R.M.S. did the experiments. M.D., N.D., and Z.-D.D. undertook bioinformatics and electromagnetic field modeling. T.D., M.T., C.D., and M.D. did the molecular biology. T.D., Z.-D.D., J.M., A.M.L., and R.M.S. analyzed the results and wrote the paper. **Competing interests:** The authors declare that they have no competing interests. **Data and materials availability:** All data needed to evaluate the conclusions in the paper are present in the paper and/or the Supplementary Materials. Additional data related to this paper may be requested from the authors.

Submitted 12 November 2018
Accepted 16 September 2019
Published 30 October 2019
10.1126/sciadv.aav9847

Citation: T. Dufor, S. Grehl, A. D. Tang, M. Doulazmi, M. Traoré, N. Debray, C. Dubacq, Z.-D. Deng, J. Mariani, A. M. Lohof, R. M. Sherrard, Neural circuit repair by low-intensity magnetic stimulation requires cellular magnetoreceptors and specific stimulation patterns. *Sci. Adv.* **5**, eaav9847 (2019).